Effects of Size Dispersion Disorder on the Charge Transport in Self-Assembled 2-D Ag Nanoparticle Arrays

K. C. Beverly, J. F. Sampaio,* and J. R. Heath†

The California NanoSystems Institute and the UCLA Department of Chemistry and Biochemistry, 603 Charles E. Young Drive East, Los Angeles, California 90095-1569

Received: June 13, 2001; In Final Form: October 31, 2001

Temperature-dependent DC transport measurements on self-assembled Ag nanoparticle monolayers have been obtained as a function of particle size distribution induced disorder. A transition temperature between the transport regimes of simple, activated transport to variable range hopping is observed to be in tune with increasing disorder of the monolayer. The overall transport behavior is described in terms of a mobility gap in the Anderson localized regime and an Efros-Shklovskii variable range hopping between localized states in the gap below some temperature characterized by the degree of disorder. From these results, we predict a true insulator−metal transition at narrow but still finite (<3%) size distributions.

Introduction

Chemically synthesized nanoparticles and quantum dots (QDs) are becoming model systems for investigating the fundamental physics[1,2] and chemistry[3] of low dimensional solids and nanoscopic materials. Scaling behavior, size and shape dependence, and quantum confinement phenomena are all areas of interest in which these systems provide a powerful and often unique environment for manipulation and investigation. A natural extension of these studies has been the exploration of the collective properties of assembled arrays of QDs.[4] The advent of synthetic techniques for preparing narrow and tunable size distributions of metal and semiconductor nanoparticles has provided building blocks for assembling ordered 2D and 3D superlattices with domain sizes on the order of hundreds of unit cells.[5,6] The nanoparticles, often passivated with organic ligands attached to their surfaces, play the role of atoms in the superlattice "artificial" solids. Several groups are now exploring properties of such QD solids, although the field remains relatively open due to the extraordinary difficulty in probing these structures in a consistent and controllable fashion. Nevertheless, reports on the transport characteristics of magnetic,[7] noble metal,[8−10] and semiconductor nanoparticle[11] arrays as well as three-dimensional metal nanoparticle superlattices[12] have appeared in the recent literature.

Over the past few years we have been investigating two-dimensional (2-D) arrays of organically passivated Ag nanoparticles that are prepared at the air−water interface of a Langmuir trough. The Langmuir compression technique, coupled with the choice of the passivating ligand, can be utilized to continuously or stepwise tune the interparticle separation distance, over the range from >20 Å to about 5 Å. These QD monolayers have been characterized using a variety of techniques including optical,[13] impedance,[14] and tunneling spectroscopies.[15] The electronic nature of the QD arrays can be tuned quite extensively through the manipulation of several fundamental variables, including particle size, interparticle separation distance, and lattice order/disorder. Notably, this control has been demonstrated in the reversible metal−insulator transition in a Langmuir monolayer of silver QDs, observed at room temperature and as a function of monolayer compression on the Langmuir trough.

We and other groups[7−9,12] have begun to investigate the temperature-dependent DC transport characteristics of 2D QD films. Such measurements are the standard for elucidating mechanistic information about transport in the solid state. In our case, we have reported on the preparation of up to six different devices from a single Langmuir monolayer of alkanethiol-passivated 7.8 (±0.6) nm Ag QDs.[10] Each device corresponded to a transfer at a different point along the pressure/area (π/A) isotherm, and thus to a different interparticle separation distance. The temperature-dependent resistance of those devices, measured over the range of ∼50 to 300 K, revealed two distinct transport regimes. For highly compressed monolayers, the films exhibited metallic conductivity (decreasing resistance (R) with decreasing temperature (T)) above ∼190 K, and simple, activated transport ($\ln(R) \propto E_\mu/T$, where E_μ is the activation energy) at lower temperatures. Throughout the activated regime, E_μ decreased steadily with lattice compression, and particles that were passivated with shorter ligands exhibited a lower E_μ for similar values of compression. In addition, the temperature of minimum resistance (T_{min})—i.e., the temperature at which the transport properties passed from metallic to insulating—decreased with decreasing E_μ. While these measurements revealed a number of trends, they opened up a number of mechanistic questions—especially as related to the importance of disorder in the transport characteristics. In this paper, we address this issue by a stepwise fine-tuning of the variable of superlattices disorder across a series of devices, while attempting to maintain similar values for the parameters of mean particle size, passivating ligand length, and lattice compression. The critical experimental handle is the width of the particle size distribution. We report on the transport properties, from 300 to ∼10 K, of six different monolayers of ∼70 Å diameter, dodecanethiol-passivated Ag QDs, in which the width of the particle size distribution was varied from 6.6% to 13.8%. Similar

* Corresponding author. E-mail: heath@chem.ucla.edu.

† On sabbatical leave. Permanent address: Universidade Federal de Minas Gerais, Depto. de Fisica, C. P. 702, CEP. 30123-970, Belo Horizonte, M. G., Brazil.

10.1021/jp012261g CCC: $22.00
Published on Web 02/12/2002

to our previous reports, all films exhibited metallic-conductivity above ~200K, and then activated transport below 200 K. However, at some lower temperature, between 30 and 100 K, a second transition (T_{cross}) was observed as the system crossed over from simple activated transport to a third regime of variable-range hopping (VRH). In the VRH regime, the power dependence of the resistance (ρ) varies as $(\ln(\rho/\rho_o) = (T_s/T)^{1/2})$. T_{cross} correlated linearly with the particle size distribution width, implying that superlattice disorder is the major variable upon which T_{cross} depends. Furthermore, the measurements extrapolate to generate a 0 K value of T_{cross} at a size distribution width of approximately 3%. We argue that these results imply that it may be possible to observe true metallic conductivity to near 0 K in a 2-D QD array, given a sufficiently narrow size distribution.

Experimental Details

Particle Synthesis. All particles were synthesized using chemicals obtained from Aldrich Chemical Co. and used without further purification unless otherwise noted. Seventy-angstrom-diameter dodecanethiol-capped Ag nanoparticles with a variable size distribution were synthesized using the method first developed by Brust et al.[16] for gold nanoparticles, and described in previous literature.[17] In short, a measured amount of $AgNO_3$ (99.999%) is dissolved in 18.2 MΩ water. In a separate flask, $(octyl)_4N^+Br^-$ is dissolved in $HCCl_3$ and added slowly to the dissolved Ag salt solution while vigorously stirring. The organic salt acts as a phase transfer reagent in the reaction. After a short period of time, allowing the resulting slurry to become uniform, dodecane thiol is added in all cases and allowed to react for a variable amount of time. In a separate beaker, $NaBH_4$ is dissolved in a small amount of 18.2 MΩ water and added rapidly to the grayish green mixture as a reductive agent. The reaction is allowed to proceed for up to 3 h. Particles are isolated by precipitation with methanol. Additional size selective precipitations are done to further narrow the size distribution if necessary. All particles are briefly sonicated in acetone to remove any excess ligand. Precise tuning of both the size and size distribution can be achieved by varying the following synthetic parameters: the amount of dodecane thiol added, the time the phase transfer reagent is allowed to stir prior to addition of the alkanethiol, and, varying the amount of time the alkanethiol is allowed to react prior to the addition of the reducing agent. Increasing the amount of the thiol added (typical range: 125−250 μL) or increasing the amount of time of either step decreases the particle size and increases the particle size distribution. Typical molar ratios for alkylthiol/$AgNO_3$/(octyl)$4N^+$-Br^-/$NaBH_4$ are 1:3:7:20 and a typical initial weight for the silver salt is ~250 mg.

Device Preparation. Dodecanethiol-capped Ag nanoparticle monolayers were prepared at the air/water interface on a Langmuir trough and transferred at the highest compression possible. For the films utilized here, categorized in terms of the size distribution widths, the numbers were 6.6% at 41 mN/m, 8% at 41 mN/m, 9% at 39 mN/m, 9.2% at 38 mN/m, 10% at 38 mN/m, and 13.8% at 39 mN/m. The transfer was to glass substrates pre-patterned with Au electrodes, using a reverse Schaeffer technique in which the glass substrate was carefully brought down into contact with the monolayer. A parallel electrode configuration was used to maximize the geometric factor and decrease the resistance in order to increase the temperature range of the measurement. The distance between the electrodes was 5 μm in all devices and the length of the electrodes covered by the monolayer varied depending on the transfer, but was between 5 and 7 μm in all films. These devices were constructed using conventional optical lithography and metal deposition by e-beam evaporation. A thin Cr (50 Å) layer was used to ensure good adhesion of the Au film (250 Å) to the glass substrate.

Transport Measurements. Temperature-dependent electrical measurements were done inside a Quantum Design MPMS XL SQUID magnetometer which provided excellent temperature control (±1%) between 2 K and 280 K and the ability to perform simultaneous magnetic measurements in fields up to 5 T, although the field measurements will not be described here. Electrical measurements were made using a Keithley 6430 Sub-Femtoamp Remote SourceMeter, a National Instruments 6036E DAQ card, and a DL Instruments 1211 Current PreAmplifier utilizing a typical 2-point or 4-point configuration.

Particle Size Distribution Measurements. Particle size distributions were measured using TEM imaging. A simple image analysis was performed on several regions of a TEM grid, each containing several hundred particles. The TEM grids were co-collected with the monolayers used for the device transport measurements, also using the same reverse Schaeffer technique. The scanned regions were collected over sufficiently large areas to ensure a statistical sampling of the film.

Results and Discussion

Six sets of ~7 nm diameter dodecanethiol ($C_{12}H_{25}SH$-passivated Ag QDs were prepared, with size distributions varying from 6.6% to 13.8%. Representative TEM micrographs and size distribution histograms of four of those monolayer films are presented in Figure 1. The average particle size across all of the films was kept nearly constant, ranging from between 67 and 75 Å. Also in Figure 1 we present Fourier transforms of the TEM images that reveal the increasing superlattice order with decreasing size distribution width. Note that the films yield a single-crystal transform pattern for the narrowest distributions, which evolves into a polycrystalline, or powder-like pattern for the 13.8% distribution width film. However, even for the narrowest size distributions, the domain sizes were only about 1 μm, which was substantially smaller than the electrode separation distance (5 μm), and so all films were, in effect, polycrystalline. The average interparticle separation distance δ (= distance between the surfaces of the metal cores of adjacent particles) was measured to be 8 ±1 Å. The films shown in Figure 1, as well as the other films discussed here, were collected from the same Langmuir monolayers, and at the same point in the π/A isotherms, as were used for the transport measurements. Both devices and TEM grids were prepared within a couple of minutes of each other. Particle size-dependent phase separation, which can occur for broad size distributions of particles, was not observed in any of these films beyond what is represented in the micrographs. All films could be re-dispersed in $HCCl_3$ after they were used. We have found this to be an excellent test of nanoparticle integrity, as effects such as Ostwald ripening of the nanoparticle arrays tend to destroy solubility.

In Figure 2 we present current−voltage traces, collected at various temperatures, for the 9% size distribution film utilized here. This type of Ohmic, or, at the lowest temperatures, nearly-Ohmic response at low bias voltages was observed for all the films. Andres' and Jaeger's groups have separately reported current−voltage curves for 2-D QD arrays for significantly larger interparticle separation distances (δ > 20 Å), and for those films, current flow near zero bias is blocked, presumably because those films are Mott insulators with a Coulomb gap that arises from the single particle charging energies. 2D QD

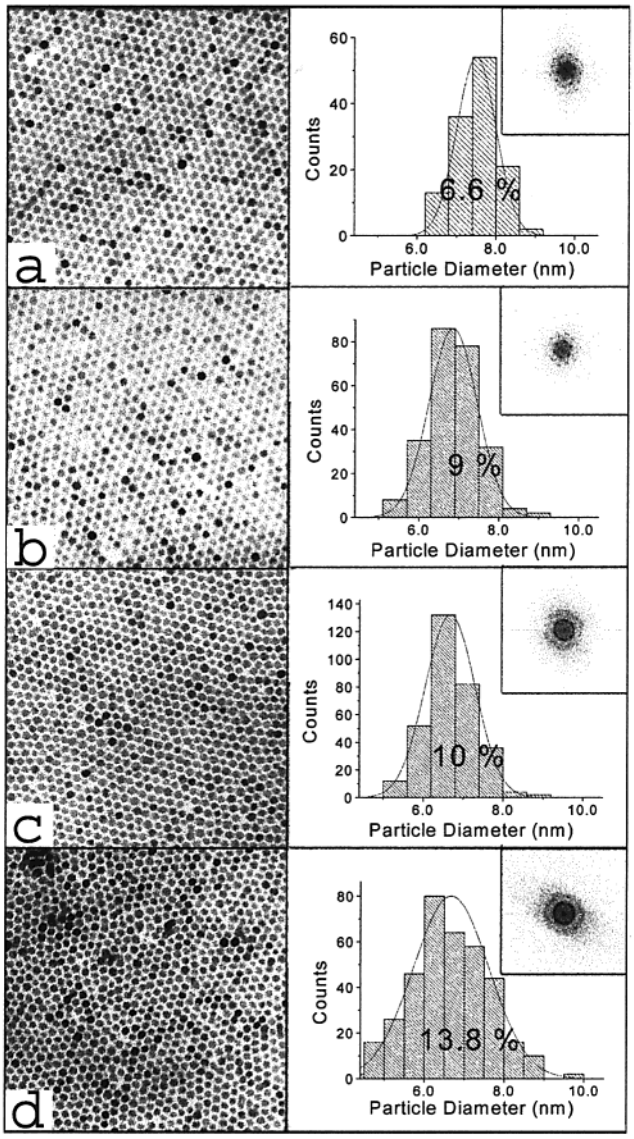

Figure 1. TEM micrographs and size distribution histograms for 4 of the QD arrays investigated here. In the above left we have included reciprocal space projections of the array as determined by a FFT of the real space TEM images. These demonstrate the transition from single-domain to poly-domain structure in these films (over the pictured length scale) as the size distribution width increases. All films were characterized by multiple domains over the length scales of the transport measurements (5 μm inter-electrode spacing). The average particle size for all distributions was around 67 Å or 68 Å, except for the 6.6% distribution width sample, which was characterized by an average size of 73 Å.

arrays have been described within the framework of a Mott−Hubbard model in which the Hubbard energy, representing the center-to-center separation between the two lowest lying bands, is given by the particle charging energy, U_c. This is the energy required to remove an electron from a charge-neutral particle and place it on another charge-neutral particle to form an unbound electron−hole pair. In the limit of large interparticle separation distances, U_c is simply twice the Coulombic charging energy of a single particle; $U_c = e^2/C$ where $C \equiv 4\pi\kappa\epsilon_o R$, and is the capacitance of the particle, e is the electronic charge, ϵ_o is the vacuum electrical permittivity, and κ is the effective dielectric constant.[18] Thus, when particles are well-separated, the array is an insulator with a Coulombic energy gap, U_g. The arrays investigated by Andres' and Jaeger's groups fall into this category.

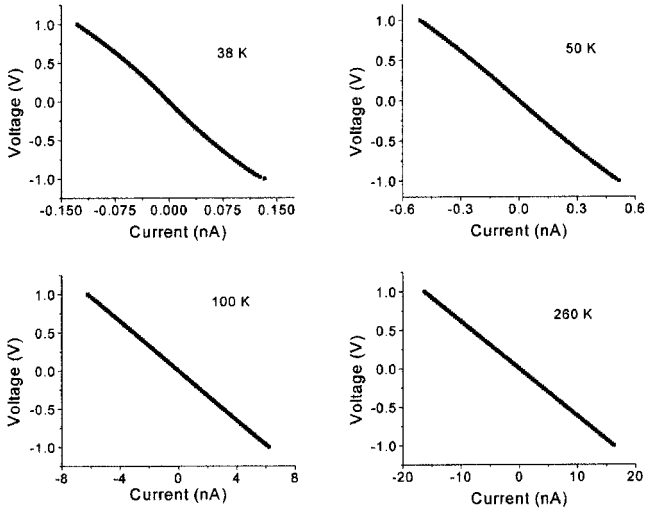

Figure 2. Current−voltage traces for the 9% size distribution QD array, taken at a few different temperatures. Note that all traces generate an ohmic response in the vicinity of zero bias.

When the interparticle separation distance (δ) is decreased, such as via compression of the Langmuir monolayer, the separation between the valence and conduction bands, or U_g, is reduced due to increasing wave function overlap. As δ becomes smaller, the interparticle exchange coupling increases and so the width of the upper and lower bands, Γ_U and Γ_L, respectively, increases. Therefore, the Coulomb gap, U_g, narrows with decreasing interparticle distance; $U_g = U_c - {}^1/_2(\Gamma_U + \Gamma_L)$, as in a normal Mott insulator. At sufficiently high compression, or more simply, when $U_c = {}^1/_2(\Gamma_U + \Gamma_L)$, the gap vanishes and the two bands merge. If the bands consist of extended states at the Fermi energy, a Mott insulator-to-metal transition is expected. However, if states are localized in this region, as would be expected in a system with some disorder, the transition will be from a Mott insulator to an Anderson localized insulator. In this case, conduction occurs via activation to the mobility edge, and therefore is characterized by an activation energy E_μ. At low temperatures, electrons condense to localized states near the Fermi energy, leading to a variable range hopping (VRH) mechanism for transport. In the VRH regime, the charge carriers must optimize the competition between distance and the number of available states when hopping from site to site.[19] If electron−electron interactions are significant, relative to the disorder, a soft gap at the Fermi energy, U_{EC}, forms and modifies the temperature dependence of the VRH.[20]

In Figure 3, we present the temperature-dependent resistance of the six films investigated here, plotting the data as $\log(R)$ vs T^{-1}. All of the films were compressed through the insulator-to-metal transition, as observed by eye. In previous work, we demonstrated that this visual change in the films correlates with the appearance of a free-electron response in the complex dielectric function (a negative-valued real component) of the film at both low (10 kHz−10 MHz)[14] and optical frequencies.[13] Consistent with those results, all films exhibited metallic-like DC conductivity at room temperature (decreasing resistance with decreasing temperature). Similar to our previous report, the temperature-dependent resistance passes through a minimum value, T_{min}, near 200 K, below which charge transport is activated. Through the activated region, the temperature-dependent resistance follows a $\log(R) = E_\mu/T$, or a T^{-1} scaling law.

At lower temperatures, deviation from simple activated behavior toward a reduced temperature dependence was ob-

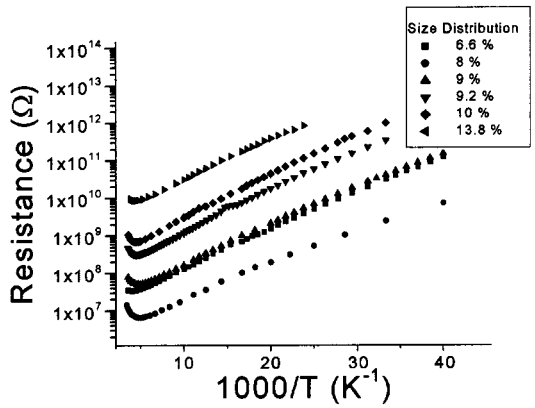

Figure 3. Plot of log(R) vs T^{-1} for the various particle size distributions. Note that all films exhibit metallic-like conductivity at the highest temperatures, with a minimum resistance value occurring at a temperature (T_{min}) near 200 K for each film. Below T $_{min}$, the transport follows a simple activated mechanism that deviates to a log-(R) $\propto T^{-1/2}$ dependence at lower temperatures.

served for all of the films. In fact, as discussed above, such a deviation is expected for any disordered system due to condensation of the carriers to the density of localized states within the mobility gap. In most disordered systems the transition is first to a dimensionally dependent Mott VRH regime that follows a $T^{-1/3}$ scaling law in 2-D. However, in all disordered systems (dimensionally independent) the Mott VRH regime is replaced by a $T^{-1/2}$ dependence, as described by Efros and Shklovskii,[20] due to electron−electron interactions that become important as the carriers are confined to fewer and fewer thermally available states.[21] In the present system, electron−electron interactions appear to be important to much higher temperatures and thus the transition is directly to the Efros−Shklovskii (ES) VRH regime. A similar behavior has been seen in at least one other system.[22] The deviation to $T^{-1/2}$ behavior, which is not very easy to detect by simple visual inspection of Figure 3, can be more readily observed in Figures 4a and 4b. In Figure 4a we plot log(R) vs $T^{-1/2}$, and we normalize the resistance of all films to each other at low T. All plots follow a $T^{-1/2}$ dependence at the lowest temperatures, and all films deviate from that behavior at higher temperatures, ranging from $T^{-1/2} = 0.17$ (∼35 K) to $T^{-1/2} = 0.1$ (∼100 K). The temperature at which the behavior crosses over from $T^{-1/2}$ to T^{-1} scaling (T_{cross}) is best extracted from the plot of Figure 4b, in which we plot d[ln(R)]/d[ln($T^{-1/2}$)] vs T. This plot should have a zero-valued slope through the $T^{-1/2}$ scaling range, deviating to positive slope after T_{cross}. Figure 4a and 4b both tell the same story: the more disordered the film, the higher the value of T_{cross}.

In Figure 5, we plot the extracted values of T_{cross} vs the particle size distribution. As can be seen from this figure, T_{cross} appears to tune linearly with δW. A key result from this work is that the extrapolation for $T_{cross} = 0$ comes at a finite particle size distribution width of about 3%, and we will come back to this result below. The dependence of the conductivity at temperatures below T_{cross} fits very well to the ES model, $\sigma_{vrh} \propto \exp\{-(T_{ES}/T)^{1/2}\}$. Here, T_{ES} is the characteristic temperature of the model, and depends on the hopping energy. T_{ES} can be related to the localization lengthscale ξ by $T_{ES} = \beta e^2/\kappa\xi$, where β is a constant, e is the fundamental unit of charge, and κ is the effective dielectric constant of the organic material that separates the metallic cores of the particles. Assuming a value of 3 for κ, ξ is found, for all films, to be in the range of 5 to 10 nm, or about the size of one or two particles.

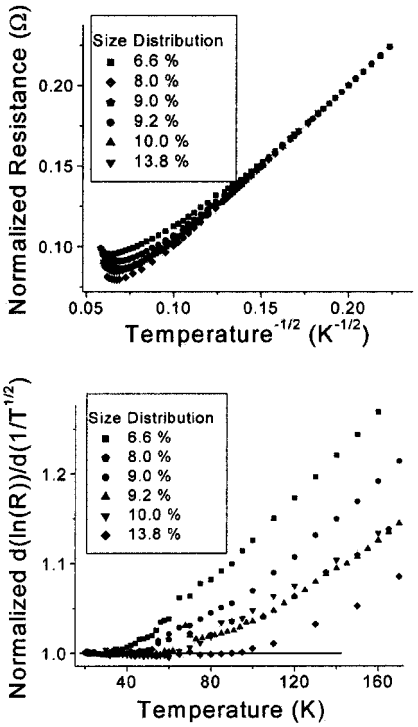

Figure 4. Two representations of the transition from the activated (T^{-1}) to the variable range hopping regime ($T^{-1/2}$) are plotted here. (a) This plot is of ln(R) vs $T^{-1/2}$ in which the measured resistance value of all films are normalized to each other at low temperatures. Deviations from linear behavior indicate a transition to the activated regime (T^{-1}). Particle size distribution width increases from top to bottom (high-temperature side of plot). (b) d(ln(R))/d(ln($T^{-1/2}$) vs T, plot, which exhibits a zero-valued slope through the variable-range-hopping ($T^{-1/2}$) regime. The particle size distribution width increases from left to right.

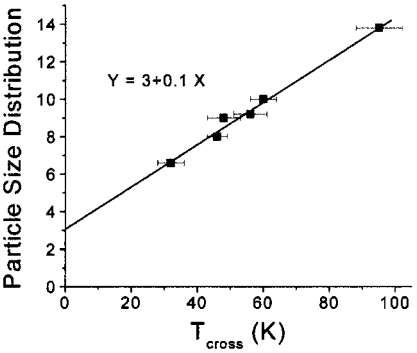

Figure 5. Plot of the particle size distribution vs the transition temperature, T_{cross}, which describes the crossover point between an activated transport mechanism (ln(R) $\propto E_a/T$ and variable-range hopping (ln(R) $\propto T^{-1/2}$). Note that T_{cross} has a 0 K value at a finite (∼3%) particle size distribution.

Within the context of the somewhat simplistic model outlined above, the manipulation of T_{cross} with particle size distribution can be construed as a probe of the density of localized states at the Fermi level or, in other words, the degree of disorder. Firm theoretical treatment of this crossover parameter is lacking in the literature because very few systems exhibit a direct transition from a simple, activated process to the ES-VRH mechanism. Instead, a Mott-type variable range hopping mechanism, MT-VRH, is more commonly seen to bridge the temperature range between a simple activated mechanism and the ES-VRH mechanism.[21] Nevertheless, the crossover temperature would depend, in some way, on the density of the localized states, although we have found neither predictions nor explanations

for a linear dependence of T_{cross} on δW. Certainly further theoretical work linking the particle size distribution-induced disorder to the density of the localized states would likely improve our understanding of the relationship seen, and might indicate whether our model system represents a general case. Nevertheless, we can put together a simple, qualitative model for transport through these highly compressed films. The fact that all films exhibit metallic-like conductivity at the highest temperatures indicates that the Coulomb gap, U_g, has closed due to strong exchange coupling between adjacent quantum dots in the arrays. However, the states near the Fermi level are those states at the edges of the conduction and valence bands, and are localized states. At energies above the Fermi level, the states are increasingly delocalized, and thermal activation to these states, or, in other words, to a mobility edge, is required for conductivity. As temperature is reduced from 300 to 200 K, the mobility of charge carriers increases (as in a metal), but the numbers of charge carriers decreases. Increasing mobility with decreasing temperature dominates this regime, and so resistance decreases with temperature. Below T_{min}, this trend reverses, and thermal activation to the mobility edge is required for charge transport. This is the activated, or T^{-1} regime. Below T_{cross}, a VRH mechanism dominates, as charge carriers get trapped in localized states. T_{cross} depends on the numbers of localized states, and so depends on the disorder of the array. However, it seems intriguing that if size distributions leading to a T_{cross} at 0 K could be produced, less than 3% in this case, then, for a similarly compressed 2-D QD superlattice such as was utilized here, the ES-VRH regime would not be present. This implies the absence of localized states, and therefore the absence of a mobility edge. The implication is that such a 2-D sample might exhibit a metal−insulator phase transition, with metallic behavior to near 0 K. This is because the value of the ratio of the bandwidth, Γ, to the energy disorder parameter, W, would be above the critical value as defined by Anderson.[23] Synthetic methods may now be available to attain such narrow size distributions[24] and we are currently working toward testing this prediction through both experiments and theoretical modeling.

In conclusion, we have presented a study of the effects of the systematic variation of particle size distribution, a significant source of disorder within the system, on the temperature-dependent transport characteristics of highly compressed Ag nanoparticle arrays prepared on a Langmuir trough and transferred to electrode patterned glass substrates. The films exhibit metallic conductivity to temperatures around 200 K, followed by activated transport which, at some low temperature, crosses over to a variable-range hopping mechanism. The crossover temperature at which the simple activated process is replaced by a variable-range hopping mechanism, appears to be highly correlated with the degree of disorder in the system. Below T_{cross}, in all films, the temperature dependence of the conductivity appears to follow $\sigma_{vrh} \propto \exp\{-(T_{ES}/T)^p\}$, in which $p = 1/2$, and is characteristic of Efros−Shklovskii variable- range hopping. We describe these results in terms of a disorder-driven Mott insulator−Anderson insulator transition. Disorder within the superlattice tends to localize the states at the Fermi energy, and forbid the observance of a Mott metal insulator transition when probed at large length scales. From these results, we predict a true insulator−metal transition at significantly narrower but still finite size distributions.

Acknowledgment. J.F.S. thanks the Brazilian agency Conselho Nacional de Desenvolvimento Cientifico e Tecnológico (CNPq) for support. This research was funded by the Department of Energy and by a CULAR grant, administered by the Regents of the University of California.

References and Notes

(1) (a) Collier, C. P.; Vossmeyer, T.; Heath, J. R. *Annu. Rev. Phys. Chem.* **1998**, *49*, 371. (b) Murray, C. B.; Kagan, C. R.; Bawendi, M. G. *Annu. Rev. Mater. Sci.* **2000**, *30*, 545.

(2) Schmid, G.; Baumle, M.; Geerkens, M.; Helm, I. *Chem. Soc. Rev.* **1999**, *28*, 179.

(3) Klimov, V. I.; Mikhailovsky, A. A.; Xu, S.; Malko, A.; Hollingsworth, J. A.; Leatherdale, C. A.; Eisler, H. J.; Bawendi, M. G. *Science* **2000**, *290*, 314.

(4) Markovich, G.; Collier, C. P.; Henrichs, S.; Remacle, F.; Levine, R.; Heath, J. R. *Acc. Chem. Res.* **1999**, *32*, 415.

(5) Murray, C. B.; Kagan, C. R.; Bawendi, M. G. *Science* **1995**, *270*, 1335.

(6) Whetten, R. L.; Khoury, J. T.; Alvarez, M. M.; Murthy, S.; Vezmar, I.; Wang, Z. L.; Stephens, P. W.; Cleveland, C. L.; Luedtke, W. D.; Landman, U. *Adv. Mater.* **1996**, *8*, 428.

(7) Black, C. T.; Murray, C. B.; Sandstrom, R. L.; Sun, S. *Science* **2000**, *290*, 1131.

(8) Andres, R. P.; Bein, T.; Dorogi, M.; Feng, S.; Henderson, J. I.; Kubiak, C. P.; Mahoney, W.; Osifchin, R. G.; Reifenberger, R. *Science* **1996**, *272*, 1323.

(9) Lin, X. M.; Jaeger, H. M.; Sorensen, C. M.; Klabunde, K. J. *J. Phys. Chem. B* **2001**, *105*, 3353.

(10) Sampaio, J. F.; Beverly, K. C.; Heath, J. R. *J. Phys. Chem. B* **2001**, *105*, 8797.

(11) Kim, S.-H.; Markovich, G.; Rezvani, S.; Choi, S. H.; Wang, K. L.; Heath, J. R. *Appl. Phys. Lett.* **1999**, *74*, 317.

(12) Doty, R. C.; Yu, H.; Shih, C. K.; Korgel, B. A. *J. Phys. Chem. B* **2001**, *105*, 8291.

(13) (a) Collier, C. P.; Saykally, R. J.; Shinag, J. J.; Henrichs, S. E.; Heath, J. R. *Science* **1997**, *277*, 1978. (b) Henrichs, S.; Collier, C. P.; Saykally, R. J.; Shen, Y. R.; Heath, J. R. *J. Am. Chem. Soc.* **2000**, *122*, 4077.

(14) Markovich, G.; Collier, C. P.; Heath, J. R. *Phys. Rev. Lett.* **1998**, *80*, 3807.

(15) Kim, S.-H.; Medeiros-Ribeiro, G.; Ohlberg, D. A. A.; Williams, Stanley R.; Heath, J. R. *J. Phys. Chem. B* **1999**, *103*, 10341; Medeiros-Ribeiro, G.; Ohlberg, D. A. A.; Williams, R. S.; Heath, J. R. *Phys. Rev. B* **1999**, *59*, 1633.

(16) Brust, M.; Walker, M.; Schiffrin, D. J.; Whyman, R. *J. Chem. Soc. Chem. Commun.* **1994**, *7*, 801.

(17) Leff, D. V.; Knobler, C. M.; Heath, J. R. *J. Phys. Chem. B* **1997**, *101*, 189.

(18) Kubo, R. *J. Phys. Soc. Jpn.* **1962**, *17*, 975.

(19) Mott, N. F. *Metal−Insulator Transitions*, 2nd ed.; Taylor & Francis: Philadelphia, 1990.

(20) Shklovskii, B. I.; Efros, A. L. *Electronic Properties of Doped Semiconductors*; Springer: New York, 1984.

(21) Schon, J. H.; Kloc, Ch.; Batlogg, B. *Phys. Rev. B* **2001**, *63*, 125304.

(22) Kim, Y.-S.; Lee, Y.-J.; Shin, H.-K. *J. Korean Phys. Soc.* **1995,** *28* (4), 505.

(23) Anderson, P. W. *Phys. Rev.* **1958**, *109*, 1492.

(24) Lin, X. M.; Sorensen, C. M.; Klabunde, K. J. *J. Nanopart. Res.* **2000**, *2*, 157.